A constitutive rheological model for agglomerating blood derived from nonequilibrium thermodynamics

Cite as: Phys. Fluids **30**, 030710 (2018); https://doi.org/10.1063/1.5016913
Submitted: 22 November 2017 . Accepted: 15 February 2018 . Published Online: 16 March 2018

Ioanna Ch. Tsimouri, Pavlos S. Stephanou, and Vlasis G. Mavrantzas

A constitutive rheological model for agglomerating blood derived from nonequilibrium thermodynamics

Ioanna Ch. Tsimouri,[1] Pavlos S. Stephanou,[1,2,a)] and Vlasis G. Mavrantzas[1,3]
[1]*Department of Chemical Engineering, University of Patras and FORTH-ICE/HT, Patras GR26504, Greece*
[2]*Department of Mathematics and Statistics, University of Cyprus, P. O. Box 20537, 1678 Nicosia, Cyprus*
[3]*Particle Technology Laboratory, Department of Mechanical and Process Engineering, Institute of Process Engineering, ETH Zurich, Sonneggstrasse 3, CH-8092 Zürich, Switzerland*

(Received 22 November 2017; accepted 15 February 2018; published online 16 March 2018)

Red blood cells tend to aggregate in the presence of plasma proteins, forming structures known as rouleaux. Here, we derive a constitutive rheological model for human blood which accounts for the formation and dissociation of rouleaux using the generalized bracket formulation of nonequilibrium thermodynamics. Similar to the model derived by Owens and co-workers ["A non-homogeneous constitutive model for human blood. Part 1. Model derivation and steady flow," J. Fluid Mech. **617**, 327–354 (2008)] through polymer network theory, each rouleau in our model is represented as a dumbbell; the corresponding structural variable is the conformation tensor of the dumbbell. The kinetics of rouleau formation and dissociation is treated as in the work of Germann *et al.* ["Nonequilibrium thermodynamic modeling of the structure and rheology of concentrated wormlike micellar solutions," J. Non-Newton. Fluid Mech. **196**, 51–57 (2013)] by assuming a set of reversible reactions, each characterized by a forward and a reverse rate constant. The final set of evolution equations for the microstructure of each rouleau and the expression for the stress tensor turn out to be very similar to those of Owens and co-workers. However, by explicitly considering a mechanism for the formation and breakage of rouleaux, our model further provides expressions for the aggregation and disaggregation rates appearing in the final transport equations, which in the kinetic theory-based network model of Owens were absent and had to be specified separately. Despite this, the two models are found to provide similar descriptions of experimental data on the size distribution of rouleaux. *Published by AIP Publishing.* https://doi.org/10.1063/1.5016913

I. INTRODUCTION

Many cardiovascular diseases leading to severe pathological conditions or even death are often associated with unusual hemodynamic behavior in the circulatory system (Yilmaz and Gundogdu, 2008). For example, intense red blood cell aggregation and hyperviscosity syndrome are observed in many pathological conditions altering the transport properties of blood (Kaliviotis *et al.*, 2017). Red blood cell (RBC) deformability is also associated with migration away from vessel walls (causing locally a depletion of erythrocytes) which can significantly affect hemodynamics. Several diseases lead to an alteration of the hemorheological behavior of blood: it is known that diabetes (Cho *et al.*, 2008), inherited sickle-cell disease (Barabino *et al.*, 2010), and malaria (Shelby *et al.*, 2003) lead to a reduction of the erythrocyte deformability and an increase of RBC aggregation, which results in an increase of blood's viscosity compared to healthy people. Obtaining therefore a deeper understanding of the factors affecting blood flow and rheology in the microvasculature clearly requires information about the effect of certain pathogens (e.g., cholesterol level, diabetes mellitus, and arterial hypertension) on blood characteristics (Yilmaz and Gundogdu, 2008). Such a development would also be highly desirable from the point of view of modeling drug transport through the circulatory system which can aid the design of improved treatments for various cardiovascular diseases associated with blood flow blockage (such as coronary artery occlusion and thrombosis) including potential diagnostic applications as pathological blood exhibits a completely different behavior than healthy blood (Yilmaz and Gundogdu, 2008 and Apostolidis and Beris, 2014).

From a rheological point of view, blood is a complex fluid consisting of blood cells suspending in a Newtonian fluid (plasma) composed mostly of water and proteins. Blood cells include RBCs, white blood cells, and platelets. Of these cells, RBCs are predominant (by ~98%), and for this reason, blood rheology is primarily determined by their behavior and direct effect on blood hemodynamics (Yilmaz and Gundogdu, 2008; Ju *et al.*, 2013; and Owens, 2006). These particulate cells have a discoidal shape and are composed of a thin elastic membrane (lipid bilayer) enclosing a hemoglobin solution, a feature that makes them considerably deformable (Yilmaz and Gundogdu, 2008 and Baskurt and Meiselman, 2003). Under physiological conditions, RBCs constitute 40%-45% of the blood volume, the so-called hematocrit (*Ht*). However, in microcirculation, *Ht* can be as low as 20% due to the smaller vessel diameters and the plasma skimming effect (Perkkiö and Keskinen, 1983).

RBCs have been experimentally observed to stick to each other spontaneously (under low flow rates) forming large column-like aggregates termed rouleaux (Merrill *et al.*, 1963a); at even lower flow rates, they form more complex,

a)Author to whom correspondence should be addressed: stefanou.pavlos@ucy.ac.cy

three-dimensional-network structures (Samsel and Perelson, 1982; 1984; Chen *et al.*, 1995; and Barshtein *et al.*, 2000). The final structure is a direct result of intercellular attractive forces that are influenced by many factors, such as the level of hematocrit (the RBC concentration), the concentration of plasma proteins (primarily fibrinogen, known to promote RBC aggregation), and several geometrical factors (e.g., the discoidal shape of RBCs, which provides a large surface area) (Chien, 1970; Merrill *et al.*, 1963b; Yilmaz and Gundogdu, 2008; and Baskurt and Meiselman, 2003). The reverse phenomenon is reported under flow, as large structures disintegrate to smaller rouleaux. Under very high flow rates, in particular, the resulting shear forces are so high that they lead to complete destruction of rouleaux; thus, only single RBCs remain.

Aggregation and disaggregation phenomena considerably affect the rheological behavior of blood: under quiescent conditions, the viscosity increases, and at certain conditions, blood exhibits a yield stress between 2 and 4 mPa (Baskurt and Meiselman, 2003) (since the network formed acts as an elastic solid below the yield stress), whilst the destruction of rouleaux under high flow rates leads to a constant Newtonian viscosity, as has been reported from both experimental investigations (Chien *et al.*, 1966; Eckmann *et al.*, 2000; and Shalak *et al.*, 1981) and coarse-grained Dissipative Particle Dynamics (DPD) simulations (Fedosov *et al.*, 2011).

Experimentally, the mechanisms that lead to the formation of rouleaux or to platelet-induced coagulation of RBCs have been studied using holographic optical tweezers (Kaestner *et al.*, 2012) and single cell force spectroscopy (Steffen *et al.*, 2013). Shiga *et al.* (1983a; 1983b) noted that strictly linear rouleaux are formed at low (7.5 s^{-1}) shear rates, each with about 10-20 RBCs, without the formation of a network. They also noted that the rouleau size follows a Poisson-like distribution. Yedgar and co-workers (Chen *et al.*, 1995 and Barshtein *et al.*, 2000) measured the rouleau dimensions in human blood at *Ht* of 10% and found small rouleaux (made up of 3–4 RBCs) at large shear rates (~67 s^{-1}) which increased to an average size of 17-32 at lower shear rates (5 s^{-1}). More recently, Mehri *et al.* (2013) measured the size of rouleaux under controlled flow conditions using an image processing approach. They found that, at small *Ht* values (5%), the rouleau size distribution was the same for two different shear rates (~5 and ~11 s^{-1}) with about 80% of RBCs belonging to rouleaux consisting of 2–6 RBCs. However, as *Ht* increased to 10% and 15%, a clear shift of the distribution to larger sizes was noted for the lower shear rate. The same conclusion was drawn from the comparison of the average rouleau size at the same shear rate at the two different *Ht* values. The average size at the lowest *Ht* was found to be the same in the two shear rates, which is consistent with the fact that low RBC concentration does not allow the formation of large rouleaux at the lower shear rates. Measurements at more physiological *Ht* conditions by Kaliviotis and co-workers (Kaliviotis, 2015; Kaliviotis and Yianneskis, 2008; and Kaliviotis *et al.*, 2011) based on optical shearing microscopy have led to an extensive characterization of the formed network based on measured values of the aggregation and aggregation integrity indices. The former describes the aggregation process (and becomes equal to one when the maximum aggregation is observed), while the latter describes the strength of the developed network (and becomes equal to one when the network strength reaches its maximum).

From a theoretical point of view, the highly complicated rheological behavior of blood has motivated the development of several non-Newtonian models to properly describe its response to an applied flow field, many of which are discussed in a review article by Yilmaz and Gundogdu (2008). The relevant constitutive models can be categorized into *time-independent* (i.e., steady-state) models and *time-dependent* models (i.e., accounting for the transient behavior of blood) (Yilmaz and Gundogdu, 2008). Although steady-state rheological models have provided a great deal of insight into the non-Newtonian behavior of blood (manifestation of shear thinning and, in many cases, of a yield stress), they are not capable of predicting elasticity or of describing the pulsatile flow conditions that blood experiences in the circulatory system. Some generalized, steady-state power-law models for systems endowed with yield stress include the Herschel-Bulkley (Herschel and Bulkley, 1926) and the Casson (Apostolidis and Beris, 2014) constitutive models, both widely used by many researchers and yielding predictions that are in good agreement with steady-state experimental data (Merrill *et al.*, 1963a; Merrill *et al.*, 1965; and Merrill and Pelletier, 1967). Recently, a generalization of these models has been proposed by Apostolidis and Beris (2014) who elegantly allowed blood viscosity and yield stress to depend on hematocrit, temperature, and fibrinogen concentration. Time-dependent constitutive models, on the other hand, can further describe the thixotropic and viscoelastic behavior of blood (in addition to shear thinning). Typical examples include the Oldroyd-B (Oldroyd, 1950) and the generalized Oldroyd-B constitutive model developed by Rajagopal and Srinivasa (Rajagopal and Srinivasa, 2000 and Anand and Rajagopal, 2004) on thermodynamic principles.

Perhaps the most sophisticated rheological model derived for blood in the last two decades is the generalized Maxwell-type model of Owens and co-workers (Owens, 2006; Fang and Owens, 2006; and Moyers-Gonzalez *et al.*, 2008), who considered blood as an ensemble of rouleaux, each rouleau modeled as an elastic dumbbell. This model was based on ideas drawn from temporary polymer network theory to account for rouleau aggregation and disaggregation. It consists of a population balance (an evolution equation for the number densities of the individual rouleau species), having the form of a general Smoluchowski coagulation equation to account for rouleau formation/dissociation, along with a differential constitutive equation for the conformation tensor of each different-sized rouleau and Kramer's expression for the extra stress tensor (Owens, 2006). Based on the experimental data of Murata and Secomb (1988), Owens and co-workers assumed an approximate relation between the aggregation rate and shear rate (Owens, 2006), independent of the rouleau size. Fang and Owens (2006) showed that the model can describe quite well the steady-state experimental data of Chien (1970). As far as transient flow experiments are concerned, only a qualitative comparison of the model was presented (Owens, 2006) against the triangular hysteresis experimental data of Bureau *et al.* (1980).

In this paper, we revisit Owens' model from the point of view of the generalized bracket formalism of nonequilibrium thermodynamics (NET) (Beris and Edwards, 1994). The generalized bracket formalism, which is considered as a single generator formalism compared to the double generator or GENERIC (general equation for the nonequilibrium reversible-irreversible coupling) formalism (Öttinger, 2004; Grmela and Öttinger, 1997; and Grmela and Öttinger, 1997), has been extensively used to model several viscoelastic fluids with a complex internal microstructure due to its capacity to describe both reversible and irreversible phenomena (Beris and Edwards, 1994; Mavrantzas and Beris, 1999a; 1999b; Beris, 2003; Stephanou *et al.*, 2009; Stephanou *et al.*, 2014; Stephanou *et al.*, 2016; Stephanou, 2015; and Stephanou, 2017). One of the advantages of the formalism is that nonequilibrium thermodynamics guarantees consistency with the 2nd law of thermodynamics. In the present work, we use nonequilibrium thermodynamics to derive a set of transport equations for blood using the same set of state variables as those employed by Owens. In addition, the evolution equations and the expression for the extra stress tensor are formally derived by considering rouleau formation and breakage through a set of aggregation/disaggregation reactions as proposed by Germann *et al.* (2013) for concentrated wormlike micellar solutions. In the context of nonequilibrium thermodynamics, we will see that flow effects on aggregation and disaggregation rates arise naturally and are modeled self-consistently. Of course, this is not the first time that rouleau formation and breakage are modeled as reversible reactions. Samsel and Perelson (1982; 1984) many years ago had proposed a kinetic model for blood including rouleau formation and dissociation based on a set of reversible reactions, each characterized by a forward and a reverse rate constant.

The rest of the paper is organized as follows: in Sec. II, we present the derivation of the new constitutive model and the evolution equations for the hydrodynamic and structural variables. Section III includes a comparison of the new model with the earlier, kinetic theory-based, model of Owens and co-workers. Section IV provides the governing equations in the non-dimensional form and a detailed description of the model parameters and their determination. Asymptotic expressions of the viscometric functions in a steady shear flow in the limit of low deformation rates, as well as of the storage and loss moduli in the case of small-amplitude oscillatory flow (SAOF), can be found in Sec. V. Section VI discusses the parameterization of the new model and presents predictions for the effect of shear on the size distribution of rouleaux which are then qualitatively compared with the results of the DPD simulations of Fedosov *et al.* (2011) and the experimental measurements of Mehri *et al.* (2013). The paper concludes with a summary of our work and a brief discussion of future plans in Sec. VII.

II. NONEQUILIBRIUM THERMODYNAMICS MODELING OF BLOOD RHEOLOGY

A. The vector of state variables

We identify $N + 1$ components, the solvent (plasma) which is denoted by the subscript s and the N rouleau species which we categorize according to their size; the smallest rouleau consists of just one RBC. Following Moyers-Gonzalez *et al.* (2008), each rouleau is modeled as an elastic dumbbell and participates in reversible reactions leading to larger or smaller rouleaux. We consider a homogeneous flow and neglect non-local diffusive effects so that all fluid components move with the same velocity $\boldsymbol{\upsilon}$. We also assume that the total system is incompressible and isothermal. For each rouleau species i ($i = 1, \ldots, N$), the following primary variables are defined: the mass density ρ_i, the momentum density $\mathbf{m}^{(i)} = \rho_i \boldsymbol{\upsilon}^{(i)}$, where $\boldsymbol{\upsilon}^{(i)} = \boldsymbol{\upsilon}$ is its velocity ($\boldsymbol{\upsilon}$ is the total velocity field), and the conformation tensor density $\mathbf{C}^{(i)}$ defined as $\mathbf{C}^{(i)} = n_i \int \mathbf{qq}\psi_i(\mathbf{q}, t)\, d^3\mathbf{q}$, i.e., as the second moment of the distribution function $\psi_i(\mathbf{q}, t)$ for the end-to-end connector vector $\mathbf{q}$ of rouleau species i (see Fig. 1).

The number density and the mass density of each rouleau species i are related through $n_i = (\rho_i/M_i)N_{Av}$, where M_i denotes the molecular weight of rouleau species i and N_{Av} is the Avogadro constant. Overall, the vector $\mathbf{x}$ of state variables is expressed as $\mathbf{x} = \left\{\mathbf{m}^{(i)}, \mathbf{C}^{(i)}, \rho_i, \mathbf{m}^{(s)}, \rho_s\right\}$, $i = 1, ..., N$. Since we consider an incompressible and isothermal system, the total mass density $\rho_{tot} = \rho_s + \sum_{i=1}^{N} \rho_i$ and the entropy density s are no longer variables of interest.

B. The Hamiltonian of the system

Within the generalized bracket formalism of nonequilibrium thermodynamics, the general evolution equation for an arbitrary functional F is postulated to be given by the following master equation (Beris and Edwards, 1994 and Beris, 2003):

$$\frac{dF}{dt} = \{F, H_m\} + [F, H_m], \tag{1}$$

where {..,..} denotes the Poisson and [..,..] denotes the dissipation bracket, and H_m is the mechanical part of the system's Hamiltonian (i.e., its total energy). H_m plays the role of the single generator of the formalism as opposed to the more general, double generator, formalism of GENERIC (Öttinger, 2004). The particular formulation accounts for both conservative (through the Poisson bracket) and dissipative (through the dissipation bracket) dynamics. Except for cases where the microstructure of the system is described by a distribution

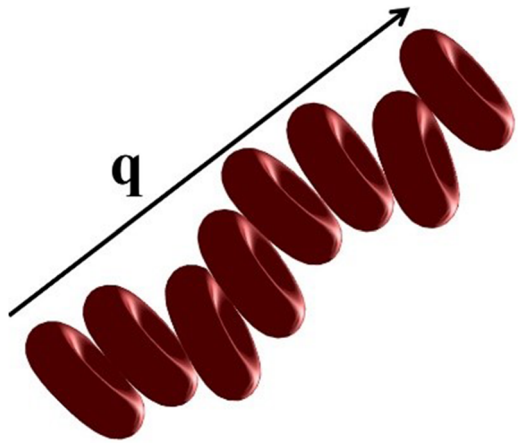

FIG. 1. Schematic representation of a rouleau and its corresponding end-to-end vector $\mathbf{q}$.

function, the single- (Beris and Edwards, 1994) and double-generator (Öttinger, 2004; Grmela and Öttinger, 1997; and Öttinger and Grmela, 1997) formalisms are equivalent and can be used interchangeably.

In the present case, the mechanical part of the system's Hamiltonian is given by the following form:

$$H_m = K_{en}(\mathbf{x}) + A(\mathbf{x}), \tag{2a}$$

$$K_{en}(\mathbf{x}) = \int \left(\frac{\mathbf{m}^{(s)} \cdot \mathbf{m}^{(s)}}{2\rho_s} + \sum_{k=1}^{N} \frac{\mathbf{m}^{(k)} \cdot \mathbf{m}^{(k)}}{2\rho_k} \right) dV, \tag{2b}$$

$$\begin{aligned} A(\mathbf{x}) &= \int a(\mathbf{x}) dV \\ &= \int \frac{1}{2} \left[\sum_{i=1}^{N} \left(K_i tr\mathbf{C}^{(i)} - \frac{\rho_i RT}{M_i} \ln \det \left(\frac{M_i K_i \mathbf{C}^{(i)}}{\rho_i RT} \right) \right) \right] dV \\ &\quad + RT \int \left[\frac{\rho_s}{M_s} \ln \left(\frac{\rho_s}{\rho} \right) + \sum_{i=1}^{N} \frac{\rho_i}{M_i} \ln \left(\frac{\rho_i}{\rho} \right) \right] dV. \end{aligned} \tag{2c}$$

In Eq. (2), $K_{en}(\mathbf{x})$ represents the kinetic energy of the system (the plasma and the N rouleau species) given by Eq. (2b) and $A(\mathbf{x})$ represents the system's Helmholtz free energy. The first integral in the second equality of Eq. (2c) expresses the sum of the elastic energies of the Hookean springs of the N rouleau species, whilst the second integral expresses the ideal Flory-Huggins entropy of mixing of the different species (rouleaux and plasma). In Eq. (2c), K_i is the Hookean spring constant of the i-species, R is the gas constant, and T is the absolute temperature.

C. The Poisson and the dissipation brackets

For systems whose internal structure is described by a conformation tensor, the expression for the Poisson bracket is well known [see, e.g., Beris and Edwards (1994) and Germann *et al.* (2013)] and is given in the supplementary material. The same holds for the dissipation bracket; its form is very similar to that used by Germann *et al.* (2013) and is discussed in detail in the supplementary material. It contains terms accounting for: (a) conformational relaxation effects for each of the N rouleaux species, (b) viscous dissipation of the solvent, which expresses the Newtonian nature of plasma, and (c) the set of reversible reactions (Germann *et al.*, 2013 and Beris and Edwards, 1994) used to describe rouleau aggregation and disaggregation. These reactions have the form

$$\begin{aligned} &A_N \underset{c_N^+}{\overset{c_N^-}{\rightleftarrows}} 2A_{N-1}, \\ &A_{i+1} \underset{c_{i+1}^+}{\overset{c_{i+1}^-}{\rightleftarrows}} 2A_i \underset{c_i^+}{\overset{c_i^-}{\rightleftarrows}} 4A_{i-1}, i = \{2, \ldots, N-1\}, \\ &A_2 \underset{c_2^+}{\overset{c_2^-}{\rightleftarrows}} 2A_1, \end{aligned} \tag{3}$$

with A_k representing a rouleau with 2^{k-1} RBCs; as a result, with A_1, we identify the rouleau species that consist of just one RBC, with A_2 the rouleau species that consist of 2 RBCs, with A_3 the rouleau species that consist of 4 RBCs, and so forth until A_N which represents the rouleau species consisting of 2^{N-1} RBCs. The rouleau species A_N corresponds to the largest agglomerates in our model.

In Eq. (3), the forward reaction represents disaggregation of one rouleau to two rouleaux, each one with half the number of RBCs of the original rouleau. In complete analogy, the reverse direction represents the aggregation of two rouleaux of equal size to one new rouleau with twice the size of the two original rouleaux. In reality, the aggregation and disaggregation mechanisms will be considerably more complicated than described here, in the sense that one can think of many different combinations of rouleau sizes that can lead to a new rouleau of a given size and vice versa. This is because the dissipation bracket associated with the irreversible dynamics of reactions, Eq. (S2) in the supplementary material, may not be correct when we have multiple reactants and products (Germann *et al.*, 2013).

How the set of reactions is treated in the context of nonequilibrium thermodynamics has been presented in detail by Germann *et al.* (2013) and for reasons of completion is also explained in the supplementary material.

D. The resulting evolution equations

Following the standard procedure (Beris and Edwards, 1994), i.e., by using the master equation, Eq. (1), and the two brackets described in the supplementary material, Eqs. (S1) and (S2), along with the fundamental building blocks [the mechanical part of the Hamiltonian, H_m, given by Eq. (2) and the tensors $\mathbf{\Lambda}^{(ii)}$ and $\mathbf{Q}$ given by Eqs. (S9) and (S10) of the supplementary material], the following time evolution equations for the number density and the conformation tensor of each rouleau species and for the total momentum density are derived, including the expression defining the total extra stress tensor:

$$\frac{Dn_i}{Dt} \equiv \frac{\partial n_i}{\partial t} + \nabla \cdot (\mathbf{v} n_i) = 2c_{i+1}^- n_{i+1} - c_{i+1}^+ n_i^2 - c_i^- n_i + \frac{1}{2} c_i^+ n_{i-1}^2, \tag{4a}$$

$$\frac{\partial n_s}{\partial t} + \nabla \cdot (\mathbf{v} n_s) = 0, \tag{4b}$$

$$\begin{aligned} \dot{\mathbf{C}}_{[1]}^{(i)} &\equiv \frac{\partial \mathbf{C}^{(i)}}{\partial t} + \mathbf{v} \cdot \nabla \mathbf{C}^{(i)} - (\nabla \mathbf{v})^T \cdot \mathbf{C}^{(i)} - \mathbf{C}^{(i)} \cdot \nabla \mathbf{v} \\ &= -\frac{1}{\lambda_i} \left(\mathbf{C}^{(i)} - \frac{n_i k_B T}{K_i} \boldsymbol{\delta} \right) + c_{i+1}^- \mathbf{C}^{(i+1)} - c_{i+1}^+ n_i \mathbf{C}^{(i)} \\ &\quad - c_i^- \mathbf{C}^{(i)} + c_i^+ n_{i-1} \mathbf{C}^{(i-1)}, \end{aligned} \tag{5}$$

$$\rho_{tot} \frac{\partial \mathbf{v}}{\partial t} = -\rho_{tot} \mathbf{v} \cdot \nabla \mathbf{v} - \nabla \cdot P + \nabla \cdot \boldsymbol{\sigma}, \tag{6a}$$

$$\begin{aligned} P &= \sum_{i=1}^{N} \left(\rho_i \frac{\delta H_m}{\delta \rho_i} + \mathbf{C}^{(i)} : \frac{\delta H_m}{\delta \mathbf{C}^{(i)}} \right) - a(\mathbf{x}), \\ \boldsymbol{\sigma} &= \sum_{i=1}^{N} \boldsymbol{\sigma}^{(i)} + \eta_s \dot{\boldsymbol{\gamma}}, \\ \boldsymbol{\sigma}^{(i)} &= K_i \mathbf{C}^{(i)} - n_i k_B T \boldsymbol{\delta}. \end{aligned} \tag{6b}$$

Equation (4a) describes the evolution equation for the number density of rouleau species i, $i = 1, \ldots, N$, involving convective effects and aggregation and disaggregation phenomena in terms of the reversible reactions considered in Eq. (3). On the other hand, the evolution equation for the solvent number

density, Eq. (4b), includes only convective effects. Note also that the total number of RBCs, $n_{tot} = \sum_{i=1}^{N} 2^{i-1} n_i$, is constant due to mass conservation. From the total number of RBCs, we can then calculate the hematocrit as $Ht = n_{tot} V_e$, where $V_e \approx 90\,\mu\text{m}^3$ is the volume of a single RBC, also known as the Mean Corpuscular Volume (MCV). Equation (5) expresses the dynamics of the conformation tensor of rouleau species i; the first term on the right-hand side refers to the relaxation toward the equilibrium value, while all other terms account for RBC aggregation and disaggregation. In Eq. (4a), note the definition of the material time derivative and in Eq. (5) the definition of the upper-convected Maxwell time derivative. Finally, Eq. (6a) is the Cauchy momentum balance equation with $\boldsymbol{\sigma}$ being the total extra stress tensor and P being the thermodynamic pressure given by Eq. (6b), $\boldsymbol{\delta}$ being the unit tensor, and $\dot{\boldsymbol{\gamma}}$ being the rate-of-strain tensor.

An important feature of our formalism is that it also leads to a closed set of analytical expressions for the reaction rates $c_i^{\pm}$, $i = 2, \ldots, N$, governing rouleau formation and dissociation in terms of the reaction fluxes and the corresponding affinities,

$$c_i^- = c_{i,eq}^- \exp\left(\frac{tr\boldsymbol{\sigma}^{(i)}}{2n_i k_B T}\right)\left[\det\left(\frac{K_i \mathbf{C}^{(i)}}{n_i k_B T}\right)\right]^{-1/2}, \tag{7a}$$

$$c_i^+ = c_{i,eq}^+ \exp\left(\frac{tr\boldsymbol{\sigma}^{(i-1)}}{n_{i-1} k_B T}\right)\left[\det\left(\frac{K_{i-1} \mathbf{C}^{(i-1)}}{n_{i-1} k_B T}\right)\right]^{-1}, \tag{7b}$$

where k_B is the Boltzmann constant and $c_{i,eq}^{\pm}$ are the aggregation and disaggregation rates at equilibrium (with the convention that $c_1^{\pm} = c_{N+1}^{\pm} = 0$).

In our work, the equilibrium aggregation and disaggregation rates are free parameters. However, it would be more appropriate to have the equilibrium rates dependent on hematocrit and fibrinogen concentration. At equilibrium, $\mathbf{C}_{eq}^{(i)} = \left(n_{i,eq} k_B T / K_i\right)\boldsymbol{\delta}$ and $n_i = n_{i,eq}$, $i = 1, \ldots, N$, with the various species number densities related through $n_{i,eq} = \frac{1}{2}\left(c_{i,eq}^+ / c_{i,eq}^-\right) n_{i-1,eq}^2$, $i = 2, \ldots, N$.

As a last remark, we mention that, in contrast to the Owens work, despite the fact that Eqs. (4) and (5) are linear, we cannot write down explicitly an evolution equation for the total extra stress tensor since the aggregation and disaggregation rates depend on the conformation tensor of each species.

III. COMPARISON OF THE NEW MODEL WITH THE KINETIC THEORY-BASED MODEL OF OWENS AND CO-WORKERS

It is of great interest to analyze how the new rheological model as derived in the context of the generalized bracket formalism of nonequilibrium thermodynamics compares with the model obtained by Owens and collaborators through polymer kinetic theory. First of all, we note that Owens' model is more complicated than ours since it allows for rouleaux of different sizes to aggregate and the same for the disaggregation mechanism: it allows for a single rouleau to break down to two different-sized rouleaux (Owens, 2006; Fang and Owens, 2006; and Moyers-Gonzalez *et al.*, 2008). But we can constraint or simplify the Owens model to include only those species that are permitted by Eq. (3), in which case we can make a one-to-one comparison of the two models; we will call this the *modified Owens* model. Then, we observe the following:

(a) In the modified Owens model, the evolution equations for the number densities of the various rouleau species are given by

$$\left.\frac{Dn_1}{Dt}\right|_{Owens} = F_{1,1} n_2 - K_{1,1} S_{1,1} (n_1)^2, \tag{8a}$$

$$\left.\frac{Dn_i}{Dt}\right|_{Owens} = \frac{1}{2} K_{i-1,i-1} S_{i-1,i-1} (n_{i-1})^2 + F_{i,i} n_{i+1} - \frac{1}{2} F_{i-1,i-1} n_i - K_{i,i} S_{i,i} (n_i)^2, \quad i = 2, \ldots, N-1, \tag{8b}$$

$$\left.\frac{Dn_N}{Dt}\right|_{Owens} = \frac{1}{2} K_{N-1,N-1} S_{N-1,N-1} (n_{N-1})^2 - \frac{1}{2} F_{N-1,N-1} n_N. \tag{8c}$$

Here, as in Owens (2006), Fang and Owens (2006), and Moyers-Gonzalez *et al.* (2008), $K_{i,j} S_{i,j}$ expresses the aggregation rate between an i-mer and a j-mer and $F_{i,j}$ expresses the rate at which an i-mer and a j-mer are formed from the breakup of an $(i+j)$-mer (following Owens' terminology, a rouleau with i RBCs is called an i-mer). In our nonequilibrium thermodynamics model, and given that $c_1^{\pm} = c_{N+1}^{\pm} = 0$, the corresponding equations, Eqs. (4), are re-written as

$$\left.\frac{Dn_1}{Dt}\right|_{new} = 2c_2^- n_2 - c_2^+ n_1^2, \tag{9a}$$

$$\left.\frac{Dn_i}{Dt}\right|_{new} = \frac{1}{2} c_i^+ n_{i-1}^2 + 2c_{i+1}^- n_{i+1} - c_i^- n_i - c_{i+1}^+ n_i^2, \quad i = 2, \ldots, N-1, \tag{9b}$$

$$\left.\frac{Dn_N}{Dt}\right|_{new} = \frac{1}{2} c_N^+ n_{N-1}^2 - c_N^- n_N. \tag{9c}$$

With the correspondence, therefore,

$$2c_i^- \to F_{i-1,i-1}; \quad c_i^+ \to K_{i-1,i-1} S_{i-1,i-1}, \quad i = 2, \ldots, N, \tag{10}$$

the two sets of equations (ours and the modified Owens ones) match identically which is very pleasing.

(b) We can proceed in the same way and compare the evolution equations for the conformation tensors. Regarding the modified Owens model, from Eq. (10), we obtain

$$\dot{\mathbf{C}}^{(1)}_{[1]}\Big|_{Owens} = -\frac{1}{\lambda_1}\left(\mathbf{C}^{(1)} - \frac{n_1 k_B T}{K_1}\boldsymbol{\delta}\right) + \underline{c_2^- n_2 \frac{k_B T}{K_2}\boldsymbol{\delta}} - c_2^+ n_1 \mathbf{C}^{(1)}, \tag{11a}$$

$$\dot{\mathbf{C}}^{(i)}_{[1]}\Big|_{Owens} = -\frac{1}{\lambda_i}\left(\mathbf{C}^{(i)} - \frac{n_i k_B T}{K_i}\boldsymbol{\delta}\right) + \underline{c_{i+1}^- \frac{n_{i+1} k_B T}{K_{i+1}}\boldsymbol{\delta} + c_i^+ (n_{i-1})^2 \frac{k_B T}{K_{i-1}}\boldsymbol{\delta}} - c_{i+1}^+ n_i \mathbf{C}^{(i)} - c_i^- \mathbf{C}^{(i)},\ i = 2, .., N-1, \tag{11b}$$

$$\dot{\mathbf{C}}^{(N)}_{[1]}\Big|_{Owens} = -\frac{1}{\lambda_N}\left(\mathbf{C}^{(N)} - \frac{n_N k_B T}{K_N}\boldsymbol{\delta}\right) + \underline{c_N^+ (n_{k-1})^2 \frac{k_B T}{K_{N-1}}\boldsymbol{\delta}} - c_N^- \mathbf{C}^{(N)}, \tag{11c}$$

which should be compared with the following expressions of our nonequilibrium thermodynamics model:

$$\dot{\mathbf{C}}^{(1)}_{[1]}\Big|_{new} = -\frac{1}{\lambda_1}\left(\mathbf{C}^{(1)} - \frac{n_1 k_B T}{K_1}\boldsymbol{\delta}\right) + \underline{c_2^- \mathbf{C}^{(2)}} - c_2^+ n_1 \mathbf{C}^{(1)}, \tag{12a}$$

$$\dot{\mathbf{C}}^{(i)}_{[1]}\Big|_{new} = -\frac{1}{\lambda_i}\left(\mathbf{C}^{(i)} - \frac{n_i k_B T}{K_i}\boldsymbol{\delta}\right) + \underline{c_{i+1}^- \mathbf{C}^{(i+1)} + c_i^+ n_{i-1} \mathbf{C}^{(i-1)}} - c_{i+1}^+ n_i \mathbf{C}^{(i)} - c_i^- \mathbf{C}^{(i)},\ i = 2, \ldots, N-1, \tag{12b}$$

$$\dot{\mathbf{C}}^{(N)}_{[1]}\Big|_{new} = -\frac{1}{\lambda_N}\left(\mathbf{C}^{(N)} - \frac{n_N k_B T}{K_N}\delta_{\alpha\beta}\right) + \underline{c_N^+ n_{N-1} \mathbf{C}^{(N-1)}} - c_N^- \mathbf{C}^{(N)}. \tag{12c}$$

We immediately notice then that the relaxation terms (first term on the right-hand side in all equations) are identical, which should be attributed to the particular form of relaxation tensors chosen in Eq. (S9) of the supplementary material for the dynamics of the individual conformation tensors. Also, identical are the resulting expressions for the extra stress tensor (although they do not include the solvent contribution). The same is true for the terms representing rouleau disaggregation (the terms with the negative sign). The terms, however, describing rouleau formation [the underlined terms in Eqs. (11) and (12)] match only when the corresponding conformation tensors are equal to their equilibrium values, $\mathbf{C}^{(i)} \sim \boldsymbol{\delta}$. This is due to the fact that, in his derivation, Owens assumed aggregation to be a Brownian process with a rate always equal to the rate under equilibrium conditions (Owens, 2006). In contrast, the new model allows for the, generally, anisotropic conformation tensor to appear in these terms, implying that these will match only under conditions close to equilibrium. Finally, in our nonequilibrium thermodynamics model, the aggregation, c_i^+, and disaggregation, c_i^-, reaction rates are given explicitly and self-consistently by Eqs. (7); in contrast, in the kinetic theory of Owens and co-workers (Owens, 2006; Fang and Owens, 2006; and Moyers-Gonzalez *et al.*, 2008), these rates must be specified externally. For example, Owens assumed that the aggregation/disaggregation processes largely confine to the end points of the rouleaux, and therefore, the corresponding rates should be independent of their size, $F_{k,j} = b(\dot{\gamma}), K_{k,j} S_{k,j} = a(\dot{\gamma})$. Although such an assumption may hold true at equilibrium, its validity under flow conditions may be questionable since we expect larger rouleaux to experience stronger hydrodynamic forces and thus to be more amenable to breakage than smaller rouleaux. In our approach, these hydrodynamic forces are explicitly taken into account through the expressions for the aggregation and disaggregation reaction rates derived in the course of the modeling approach.

IV. NON-DIMENSIONALIZATION AND MODEL PARAMETERS

In the remaining of this paper, the following dimensionalization has been used (dimensionless numbers are denoted by a tilde):

$$\begin{aligned} &\tilde{n}_i = \frac{n_i}{n_{tot}},\ \tilde{\mathbf{C}}^{(i)} = \frac{K_i \mathbf{C}^{(i)}}{n_{tot} k_B T},\ \tilde{\boldsymbol{\sigma}} = \frac{\boldsymbol{\sigma}}{n_{tot} k_B T}, \\ &\tilde{t} = \frac{t}{\lambda_N},\ \tilde{\lambda}_i = \frac{\lambda_i}{\lambda_N},\ \tilde{c}_i^+ = c_i^+ \lambda_N n_{tot},\ \tilde{c}_i^- = c_i^- \lambda_N. \end{aligned} \tag{13}$$

That is, the number densities are made dimensionless by dividing them with the total number density of RBCs; the rouleau conformation tensors are made dimensionless by multiplying them with $K_i/(n_{tot} k_B T)$ so that $\tilde{\mathbf{C}}^{(i)}_{eq} = \tilde{n}_{i,eq}\boldsymbol{\delta}$; the time and the velocity gradient are made dimensionless using the relaxation time λ_N of the largest rouleau (this, in turn, allows us to identify the dimensionless shear rate with the characteristic Weissenberg number, $\mathrm{Wi} = \dot{\gamma}\lambda_N$, where $\dot{\gamma} \equiv \sqrt{\frac{1}{2}\dot{\boldsymbol{\gamma}} : \dot{\boldsymbol{\gamma}}}$ is the applied shear rate), while the aggregation and disaggregation rates are made dimensionless by multiplying them with $\lambda_N n_{tot}$ and λ_N, respectively. Since also $K_i/K_{i+1} = 2$, we arrive at the following final set of governing equations in dimensionless units defining our model:

$$\frac{D\tilde{n}_1}{Dt}\Big|_{new} = 2\tilde{c}_2^- \tilde{n}_2 - \tilde{c}_2^+ \tilde{n}_1^2, \tag{14a}$$

$$\frac{D\tilde{n}_i}{Dt}\Big|_{new} = \frac{1}{2}\tilde{c}_i^+ \tilde{n}_{i-1}^2 + 2\tilde{c}_{i+1}^- \tilde{n}_{i+1} - \tilde{c}_i^- \tilde{n}_i - \tilde{c}_{i+1}^+ \tilde{n}_i^2,\quad i = 2, \ldots, N-1, \tag{14b}$$

$$\frac{D\tilde{n}_N}{Dt}\Big|_{new} = \frac{1}{2}\tilde{c}_N^+ \tilde{n}_{N-1}^2 - \tilde{c}_N^- \tilde{n}_N, \tag{14c}$$

and

$$\tilde{\mathbf{C}}^{(1)}_{[1]}\Big|_{new} \equiv -\frac{1}{\tilde{\lambda}_1}\left(\tilde{\mathbf{C}}^{(1)} - \tilde{n}_1\boldsymbol{\delta}\right) + 2\tilde{c}_2^- \tilde{\mathbf{C}}^{(2)} - \tilde{c}_2^+ \tilde{n}_1 \tilde{\mathbf{C}}^{(1)}, \tag{15a}$$

$$\tilde{\dot{\mathbf{C}}}^{(i)}_{[1]}\Big|_{new} \equiv -\frac{1}{\tilde{\lambda}_i}\left(\tilde{\mathbf{C}}^{(i)} - \tilde{n}_i\boldsymbol{\delta}\right) + \frac{1}{2}\tilde{c}^{+}_{i}\tilde{n}_{i-1}\tilde{\mathbf{C}}^{(i-1)} + 2\tilde{c}^{-}_{i+1}\tilde{\mathbf{C}}^{(i+1)} - \tilde{c}^{-}_{i}\tilde{\mathbf{C}}^{(i)} - \tilde{c}^{+}_{i+1}\tilde{n}_i\tilde{\mathbf{C}}^{(i)}, \tag{15b}$$

$$\tilde{\dot{\mathbf{C}}}^{(N)}_{[1]}\Big|_{new} \equiv -\frac{1}{\tilde{\lambda}_N}\left(\tilde{\mathbf{C}}^{(N)} - \tilde{n}_N\boldsymbol{\delta}\right) + \frac{1}{2}\tilde{c}^{+}_{N}\tilde{n}_{N-1}\tilde{\mathbf{C}}^{(N-1)} - \tilde{c}^{-}_{N}\tilde{\mathbf{C}}^{(N)}. \tag{15c}$$

To solve the above set of equations, we need to specify $3N-2$ parameters: the $2(N-1)$ equilibrium aggregation/disaggregation reaction rates $\tilde{c}^{+}_{i,eq}$ and $\tilde{c}^{-}_{i,eq}$, $i = 2,\ldots,N$, and the N characteristic relaxation times. As far as the total number of rouleau species N is concerned, we typically take it to be between 5 and 7 in order to cover the expected average rouleau size reported in the literature which ranges from 15 to about 65 (Usami *et al.*, 1975 and Kaliviotis and Yianneskis, 2011).

A very attractive feature of our model is that it can capture the distribution of the rouleau size also under equilibrium conditions (absence of flow). Indeed, from Eqs. (14), we get $\tilde{n}_{i,eq} = \left(\tilde{c}^{+}_{i,eq}/2\tilde{c}^{-}_{i,eq}\right)\tilde{n}^{2}_{i-1,eq}$ with $\tilde{n}_{1,eq}$ specified from the total mass balance of RBCs, $\sum_{i=1}^{N} 2^{i-1}\tilde{n}_{i,eq} = 1$. Of course, such an equilibrium state is meaningful at small *Ht* values because, as mentioned earlier, at large *Ht* values RBCs form a 3D-network [see Schmid Schönbein *et al.* (1968)] which is not considered in the present version of our model. From the experimental work of Szołna-Chodór *et al.* (2015), we also expect that the equilibrium aggregation/disaggregation reaction rates should depend on *Ht* (i.e., on RBC volume fraction). Finally, concerning the characteristic relaxation times needed to capture flow effects, to a first approximation, we can determine them by considering each rouleau to behave as a rigid rod. Then, following Doi and Edwards (1986), the relaxation times will increase with the third power of rouleau size, i.e., $\lambda_i/\lambda_j = 2^{3(i-j)}$, implying that $\lambda_{i+1}/\lambda_i = 8$. In this case, the total number of free parameters to be specified reduces to $2N-1$.

From the analysis just presented and given that most of our model parameters include the equilibrium aggregation and disaggregation reaction rates, it appears that the best strategy to parameterize the new model is by fitting its predictions to available data for the equilibrium size distribution of rouleaux and then to proceed by using the model to describe the same distribution under flow, which will also provide the predictions for the relevant viscometric functions. Unfortunately, a careful literature survey proves that the rouleau size distribution under equilibrium conditions is not available, not even for dilute blood suspensions. An alternative approach would be to fit available rheological measurements from SAOF experiments of blood samples with small *Ht* values to Eq. (17d) below for the storage, $G'(\omega)$, and loss, $G''(\omega)$, moduli, but such data are difficult to find in the literature since most of them refer to physiological *Ht* values. Currently, perhaps the most straightforward way to determine the equilibrium aggregation/disaggregation rates is by resorting to detailed DPD simulations such as those carried out by Fedosov *et al.* (2011).

V. ASYMPTOTIC BEHAVIOR IN STEADY STATE SHEAR

In this section, we study the asymptotic behavior of the two models (ours and the modified version of Owens' model to allow for aggregates that consist only of 2^{i-1}-mers) in the limit of small shear rates. We are mostly interested in obtaining analytical expressions for the important viscometric quantities at steady state. To this, we expand the rouleau conformation tensors up to first order in shear rate and solve the corresponding equations analytically. Given that the diagonal elements are always even functions of the applied shear-rate, each of these elements can be taken to remain equal to its equilibrium value. Because of this, the number densities also remain equal to their equilibrium values, $n_{i,eq} = \frac{1}{2}\left(c^{+}_{i,eq}/c^{-}_{i,eq}\right)n^{2}_{i-1,eq}$. Finally, the expression for the zero-shear-rate viscosity can be obtained directly from the expression for the off-diagonal elements of the various conformation tensors. Then, the final expressions from the modified Owens model are

$$C^{(i)}_{xy} = \frac{n_{i,eq}k_BT}{K_i}\frac{\dot{\gamma}\lambda_i}{1+\lambda_i\left(c^{+}_{i+1,eq}n_{i,eq} + c^{-}_{i,eq}\right)} \tag{16a}$$

and

$$\eta_0 - \eta_s = \frac{1}{\dot{\gamma}}\sum_{i=1}^{N} K_i C^{(i)}_{xy} = \sum_{i=1}^{N} n_{i,eq}k_BT\frac{\lambda_i}{1+\lambda_i\left(c^{+}_{i+1,eq}n_{i,eq} + c^{-}_{i,eq}\right)}. \tag{16b}$$

The corresponding expressions from our model are

$$C^{(i)}_{xy} = \sum_{j=1}^{N} A^{-1}_{ij}\lambda_j\frac{n_{j,eq}k_BT}{K_j} \tag{17a}$$

and

$$\eta_0 - \eta_s = \frac{1}{\dot{\gamma}}\sum_{i=1}^{N} K_i C^{(i)}_{xy} = \sum_{i=1}^{N} K_i\sum_{j=1}^{N} A^{-1}_{ij}\lambda_j\frac{n_{j,eq}k_BT}{K_j}, \tag{17b}$$

where $\mathbf{A}$ is the following tridiagonal matrix:

$$\begin{gathered} A_{1,1} = \lambda_1^{-1} + c^{+}_{2,eq}n_{1,eq}, \quad A_{1,2} = -c^{-}_{2,eq}, \\ A_{i,i-1} = -c^{+}_{i,eq}n_{i-1,eq}, \quad A_{i,i} = \lambda_\iota^{-1} + c^{-}_{i,eq} + c^{+}_{i+1,eq}n_{i,eq}, \\ A_{i,i+1} = -c^{-}_{i+1,eq}, i = 2,\ldots,N, \\ A_{N,N-1} = -c^{+}_{N,eq}n_{N-1,eq}, \quad A_{N,N} = \lambda_N^{-1} + c^{-}_{N,eq}. \end{gathered} \tag{17c}$$

A formal expression for the inverse of such a tridiagonal matrix is available by Usmani (1994).

We have also derived analytical expressions from the new model for the storage and loss moduli in the case of SAOF,

$$\begin{aligned} G''(\omega) &= \omega\sum_{i,j,k=1}^{N} A_{ij}\left(\omega^2\delta_{jk} + A^2_{jk}\right)^{-1}n_{k,eq}k_BT, \\ G'(\omega) &= \omega^2\sum_{i,j=1}^{N}\left(\omega^2\delta_{ij} + A^2_{ij}\right)^{-1}n_{j,eq}k_BT. \end{aligned} \tag{17d}$$

Clearly, the two models lead to different algebraic expressions for the relevant viscometric functions (rouleau conformation tensors and viscosity) even in the linear regime in the steady shear flow, and the same is true for the

zero-shear-rate viscosity and the storage and loss moduli. However, as we will discuss in Sec. VI, their actual predictions are not that different.

VI. RESULTS

A. Equilibrium rouleau size distribution for pre-sheared samples

Aggregation under no-flow conditions is typically studied by first breaking all aggregates after shearing the blood sample for sufficiently long time and then, once the flow has stopped, by monitoring the evolution of the rouleau size distribution. Figure 2 presents a comparison of the two models regarding the evolution of this rouleau size distribution after pre-shearing, for rouleau sizes up to 16 (corresponding to $N = 5$). At low Ht values, we do not expect any strong dependence of the disaggregation rates on the rouleau population or on Ht; thus, we can take all of them to be equal (e.g., equal to 10^{-4} in the results discussed below). For the longest relaxation time, we assumed the value $\lambda_N = 0.5$ s (implying that $\lambda_1 = \lambda_N/2^{3(N-1)} = 1.2 \times 10^{-4}$ s), i.e., equal to the value used for the comparison with the experimental data (see Sec. VI C below).

For the Owens model, we have to fix the values of the aggregation/disaggregation rates. In the following, these have been taken equal to the average value of the corresponding parameters chosen for our model; that is, we took $2a_0/b_{eq}$ in the Owens model to be equal to the average value of $c^+_{i,eq}/c^-_{i,eq}$ in our model. We made this choice so that the comparison between the two models is as fair as possible. Indeed, with this choice, when all $c^+_{i,eq}/c^-_{i,eq}$ are the same in our model, the resulting distributions of rouleau sizes from the two models coincide (see Fig. 2). We note that with the expressions employed by Owens (see Sec. C of the supplementary material), the ratio $2a_0/b_{eq}$ of aggregation and disaggregation rates is controlled by the Cross-model parameter θ. We also considered a fixed value of $\xi = 0.13$ s^m (as we did for the comparison with the experimental data, see Sec. VI C below), whereas θ was selected so that $2a_0/b_{eq}$ attains the value mentioned just above. Finally, for the relaxation time λ_H and the parameter m, we assumed the values used by Fang and Owens (2006), $\lambda_H = 0.004$ s and $m = 0.75$.

At $t = 0$, only single RBCs exist, but, as time goes on, association reactions between single cells start taking place and the curves gradually approach their equilibrium distributions. For short enough times [e.g., up to $t = 50$ s, see Fig. 2(a)], the various distributions are practically the same, favoring single RBCs and dumbbells.

At longer times [e.g., at $t = 500$ s in Fig. 2(b)], larger and larger rouleaux are formed especially for the larger $c^+_{i,eq}/c^-_{i,eq}$ values considered. In general, as the ratio $c^+_{i,eq}/c^-_{i,eq}$ increases, the relative concentration of larger rouleaux also increases. For times larger than about 5000 s, the resulting distribution is very similar to the equilibrium one (obtained for $t \to \infty$), see Fig. 2(d). Overall, the predictions of the two models are very similar, mostly due to the fact that the parameter $2a_0/b_{eq}$ in the Owens model was taken to be equal to the value of the ratio $c^+_{i,eq}/c^-_{i,eq}$ in the new model.

B. Rouleau size distribution under shear flow

Figure 3 compares the resulting rouleau size distributions from the two models under shear. These were obtained by starting from equilibrated samples and using the same sets of parameter values as before. Actually, for the new model, no further parameters had to be specified since the shear-rate dependence of the aggregation/disaggregation rates is directly contained in Eqs. (7). For the corresponding Owens model under shear, we had to provide values for the two additional parameters a_1 and $\dot\gamma_c$; again, for these, we chose the values used by Fang and Owens (2006), $a_1 = 2$ s^{-1} and $\dot\gamma_c = 5.78$ s^{-1}.

At relatively small shear rates [$\dot\gamma = 1$ s^{-1}, Fig. 3(a)], the resulting distributions from the two models are very similar; they are also very close to the equilibrium ones [Fig. 2(d)]. At larger shear rates [$\dot\gamma = 10$ s^{-1}, Fig. 3(b)], the new model predicts that all rouleaux with 16 red blood cells are destroyed and the sample contains mostly (up to ~50%) rouleaux with 8 red blood cells. We also observe that as $c^+_{i,eq}/c^-_{i,eq}$ decreases, the peak of the distribution decreases and the distribution favors more and more rouleaux containing 4 RBCs. Owens' model, on the other hand, predicts a weaker shear-rate dependence of the rouleau size distribution since the population of the larger rouleaux (albeit decreasing) remains approximately equal to the population of rouleaux with sizes 4 and 8 RBCs. Upon further increasing the shear rate, both models correctly predict that the peak of the size distribution is shifted to smaller rouleau sizes. As a general remark, Owens' model predicts smaller concentrations for all rouleau sizes which must be due to the assumption that the shear-rate dependence of the association and dissociation rates is the same (irrespective of the size of rouleau); in contrast, in the new model, each rouleau is characterized by its own association and dissociation rates whose dependence on the shear rate is dictated by its size.

C. Comparison with experimental data and DPD simulations

In this section, we provide a preliminary, qualitative comparison of the predictions of the new model (and of the modified Owens model) with the experimental data of Mehri *et al.* (2013) who analyzed RBC aggregates under controlled flow conditions at three different Ht values using an image processing approach. We also provide some qualitative comparison with the results of Fedosov *et al.* (2011) who studied aggregation/disaggregation phenomena under flow conditions with DPD simulations for a system with $Ht = 10\%$.

The comparison of the two models with the experimental data of Mehri *et al.* (2013) for the rouleau size distribution is shown in Fig. 4. The results refer to two different Ht values and to two different sets of shear rates. The predictions of the new model in Fig. 4(a) have been obtained for the following set of parameter values: $N = 5$, $\lambda_N = 0.5$ s, $\tilde c^+_{2,eq} = 5.2 \times 10^{-4}$, $\tilde c^+_{3,eq} = 7.6 \times 10^{-4}$, $\tilde c^+_{4,eq} = 2.8 \times 10^{-4}$, $\tilde c^+_{5,eq} = 5.3 \times 10^{-4}$, and $\tilde c^-_{i,eq} = 10^{-4}$. The corresponding data in Fig. 4(b) have been obtained for $N = 5$, $\lambda_N = 0.5$ s, $\tilde c^+_{2,eq} = 3.9 \times 10^{-4}$, $\tilde c^+_{3,eq} = 7\times10^{-4}$, $\tilde c^+_{4,eq} = 6\times10^{-4}$, $\tilde c^+_{5,eq} = 10^{-3}$, and $\tilde c^-_{i,eq} = 10^{-4}$. Both models compare well with the experimental data over the

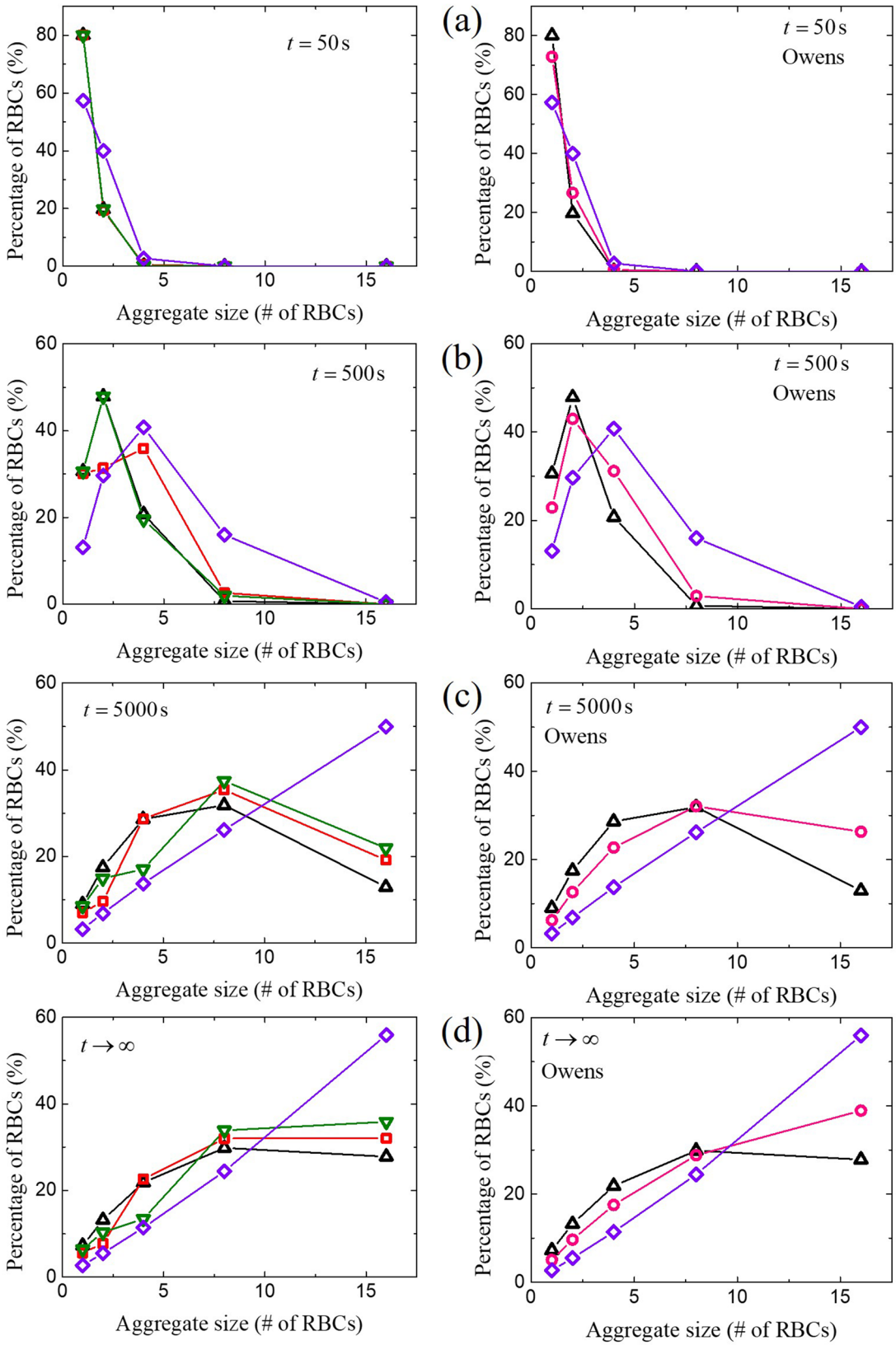

FIG. 2. Predictions of the new model compared to that of Owens presented here for the rouleau size distribution under equilibrium conditions starting from a pre-sheared sample for the following times: (a) $t = 50$ s, (b) $t = 500$ s, (c) $t = 5000$ s, and (d) steady-state. For the new model (left column), the results have been obtained by keeping $c^-_{i,eq}$ constant, equal to $c^-_{i,eq} = 10^{-4}$, $\forall i$, and changing the value of $c^+_{i,eq}$. Thus, black symbols correspond to $c^+_{i,eq} = 2.5 \times 10^{-3}$ $\forall i$, red to $c^+_{3,eq} = 7.5 \times 10^{-3}$ and $c^+_{i,eq} = 2.5 \times 10^{-3}$ $\forall i \neq 3$, green to $c^+_{4,eq} = 7.5 \times 10^{-3}$ and $c^+_{i,eq} = 2.5 \times 10^{-3}$ $\forall i \neq 4$, and purple to $c^+_{i,eq} = 7.5 \times 10^{-3}$ $\forall i$. For the Owens model, black symbols correspond to $2a_0/b_{eq} = 25$, pink to $2a_0/b_{eq} = 37.5$, and purple to $2a_0/b_{eq} = 75$.

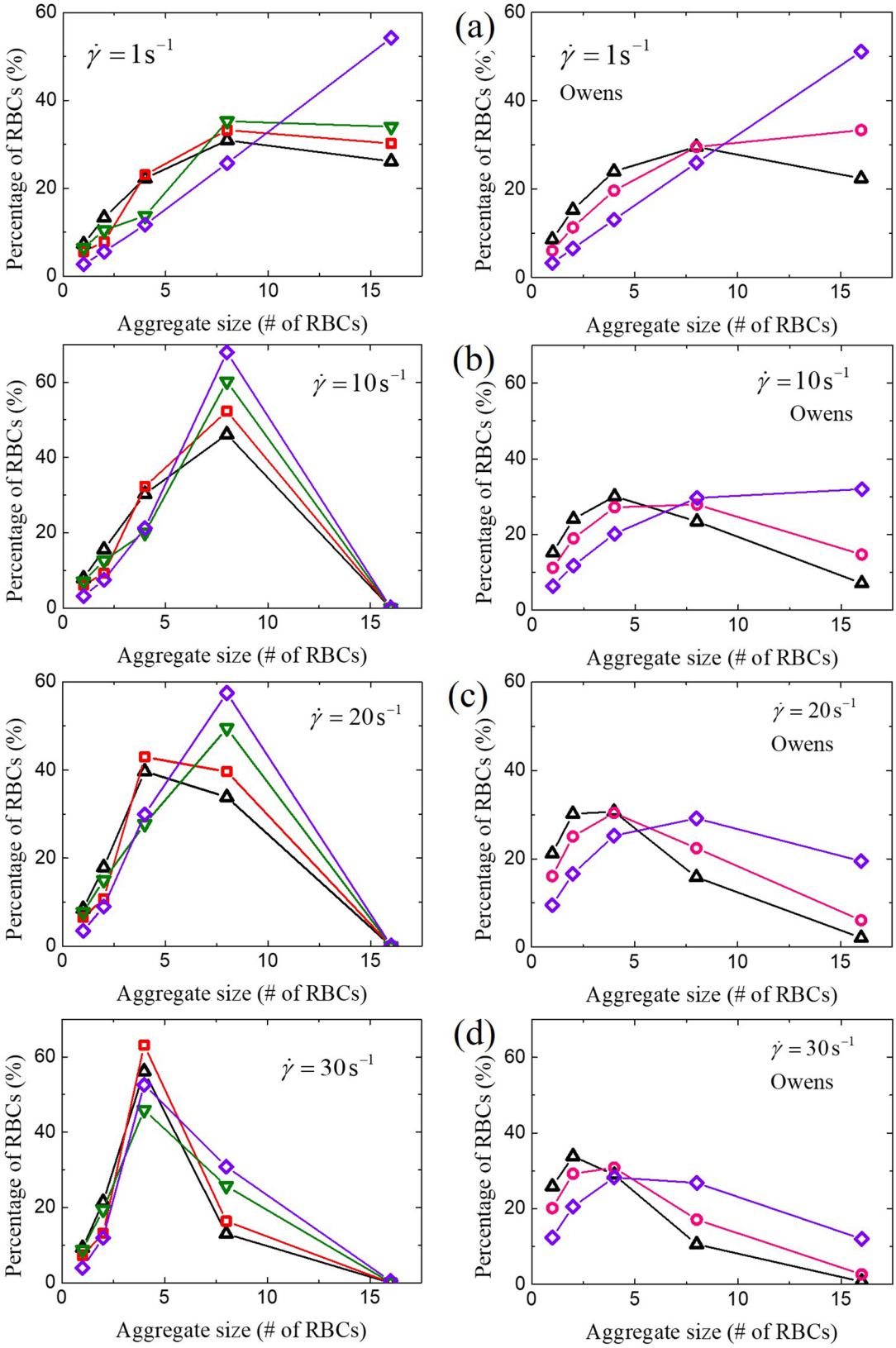

FIG. 3. Evolution of rouleau size distribution from the two models under shear starting from an equilibrated sample, for the following shear rates: (a) $\dot{\gamma} = 1\ \mathrm{s}^{-1}$, (b) $\dot{\gamma} = 10\ \mathrm{s}^{-1}$, (c) $\dot{\gamma} = 20\ \mathrm{s}^{-1}$, and (d) $\dot{\gamma} = 30\ \mathrm{s}^{-1}$. The same parameter values as in Fig. 2.

entire range of rouleau sizes studied. In more detail, for the sample with $Ht = 5\%$, we note that the new model correctly predicts both the peak of the distribution and the extent of the tail at the two shear rates. For the sample with $Ht = 10\%$, the model overestimates somewhat the peak at small shear rates, but the overall behavior is again very satisfactory.

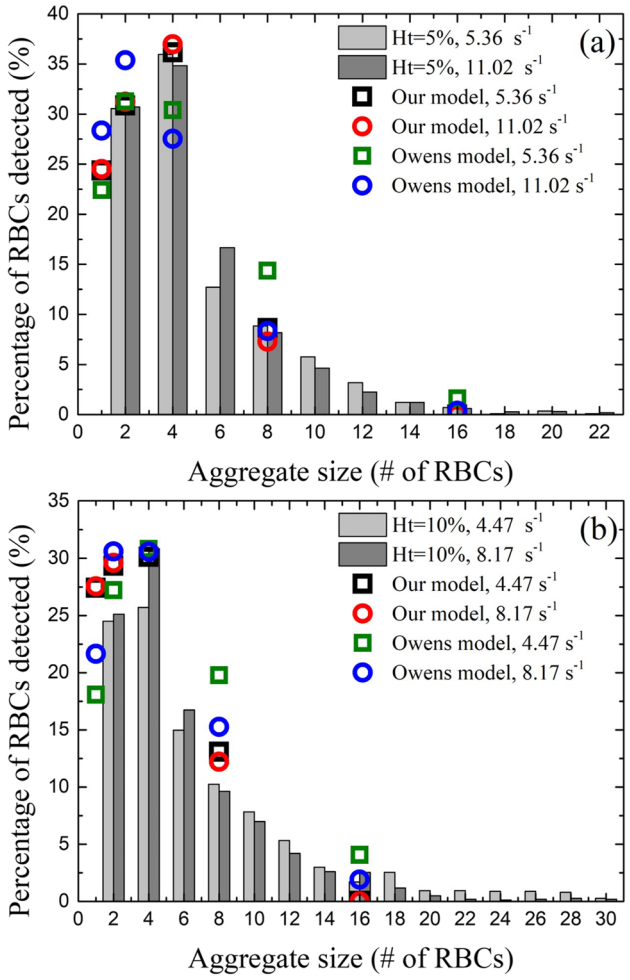

FIG. 4. Comparison of the two models with the experimental data of Mehri *et al.* (2013) for the rouleau size distribution: (a) $Ht = 5\%$ and $\dot{\gamma} = 5.36$ and 11.02 s^{-1}, and (b) $Ht = 10\%$ and $\dot{\gamma} = 4.47$ and 8.17 s^{-1}.

A few words are in order here regarding the choice of the model aggregation and disaggregation rate constants. Since we examine low Ht values, we took all disaggregation rate constants to be the same, equal to 10^{-4}. Concerning the equilibrium aggregation rates, their values were chosen so as to ensure that at the lowest Ht value, smaller rouleaux will dominate, whereas at the highest Ht the percentage of large rouleaux will increase. To achieve this, the equilibrium aggregation rates $\tilde{c}^{+}_{2,eq}$ and $\tilde{c}^{+}_{3,eq}$ of the smaller rouleaux had to be smaller in the case of the smaller Ht compared to those in the case of the larger Ht. On the other hand, the equilibrium aggregation rates $\tilde{c}^{+}_{4,eq}$ and $\tilde{c}^{+}_{5,eq}$ of the larger rouleaux were chosen to be larger than those at the lowest Ht. The exact value of all equilibrium aggregation rates for both Ht values was fitted to the experimental data. Finally, the relaxation time λ_N of the largest rouleau species was also fitted to the experimental data and estimated to be equal to 0.5 s, which corresponds to a relaxation time of a single RBC equal to 1.2×10^{-4} s.

For the modified Owens model, the set of parameters includes $a_0, a_1, \xi, \theta, m, \dot{\gamma}_c$, and λ_H (see Sec. B of the supplementary material). In Fang and Owens (2006), these correspond to $Ht = 45\%$, which is much higher than the Ht values of interest here. Thus, for the comparison with the experimental data of Fig. 4, and in order not to bias the comparison between the two models, we decided to approximate $a_0\lambda_H$ at each Ht level with the average value of our four equilibrium aggregation rates; thus, for $Ht = 5\%$, $a_0\lambda_H = 4.18 \times 10^{-6}$, while for $Ht = 10\%$, $a_0\lambda_H = 5.38 \times 10^{-6}$. For the parameters affecting the disaggregation rates, we selected the ratio between ξ and θ such that the equilibrium disaggregation reaction rates match those predicted by our model and then made specific selections for ξ and θ to get the best fits to the experimental data. Thus, for $Ht = 5\%$, we selected $\theta = 0.047$ s^m, whilst for $Ht = 10\%$, we selected $\theta = 0.041$ s^m. As in Sec. VI, we also selected $\xi = 0.13$ s^m for both Ht values. For the rest of the parameters, we kept the values employed by Fang and Owens (2006) (see also Sec. VI), $a_1 = 2$ s^{-1}, $\dot{\gamma}_c = 5.78$ s^{-1}, $m = 0.75$, and $\lambda_H = 0.004$ s. The final results are shown in Fig. 4 and confirm that with these choices the two models provide very similar descriptions of the experimental data despite their subtle differences in the form of the corresponding constitutive equations for the conformation tensors of the various rouleau sizes.

Formation and dissociation of rouleaux have also been studied in the DPD simulations of Fedosov *et al.* (2011) for a blood sample with $Ht = 10\%$. At low shear rates ($\dot{\gamma} = 0.04$ s^{-1}), the initially dispersed RBCs showed a tendency to aggregate into large rouleaux made of up to ~20 RBCs; as the shear rate was increased to moderate values ($\dot{\gamma} = 0.4$ s^{-1}), these structures were reduced in size until at high rates ($\dot{\gamma} = 4$ s^{-1}), they were dispersed almost completely into individual RBCs. For more information, see Fig. 2 and Movies 1–3 in Fedosov *et al.* (2011). Our model predictions for $Ht = 5$ and 10% using the same model parameters as in Fig. 4 for the same shear rates (0.02, 0.4, and 4 s^{-1}) are shown in Fig. 5. The data indicate only a minor dependence on the shear rate. However, and as shown in Fig. 3, at larger shear rates, the disaggregation becomes more pronounced.

According to Fig. 5, the corresponding average aggregate sizes at the two Ht values examined ($Ht = 5\%$ and 10%) will come out to be equal (i.e., independent of the applied shear rate), corresponding approximately to 2 RBCs per rouleau. This is a direct consequence of the fact that in our model we allow only for rouleaux of specific sizes (consisting of 1, 2, 4, 8, 16, . . ., RBCs) to form. In the regime of small shear rates, the relative populations of these sizes are hardly sensitive to the applied flow. It turns out that the use of a discrete distribution prevents our model from predicting simultaneously well both the RBC distribution and the average rouleau size. Another drawback of our model is that for high enough shear rates it cannot predict the complete dissociation of rouleaux to single RBCs. The reason for this is technical: if this happened, the number densities of all other species would have been zero ($\tilde{n}_{tot} = \sum_{i=1}^{N} 2^{i-1}\tilde{n}_{i,eq} = 1$), which is not allowed by our model since in the expressions for the aggregation and disaggregation rates [see Eqs. (7)] the species number densities appear in the denominator. This explains why the average aggregate size is predicted by our model not to change with the applied shear rate for the low Ht values examined here. Replacing the discrete rouleau size distribution by a continuous one as, e.g., was done by Samsel and Perelson (1982; 1984) is among our future plans.

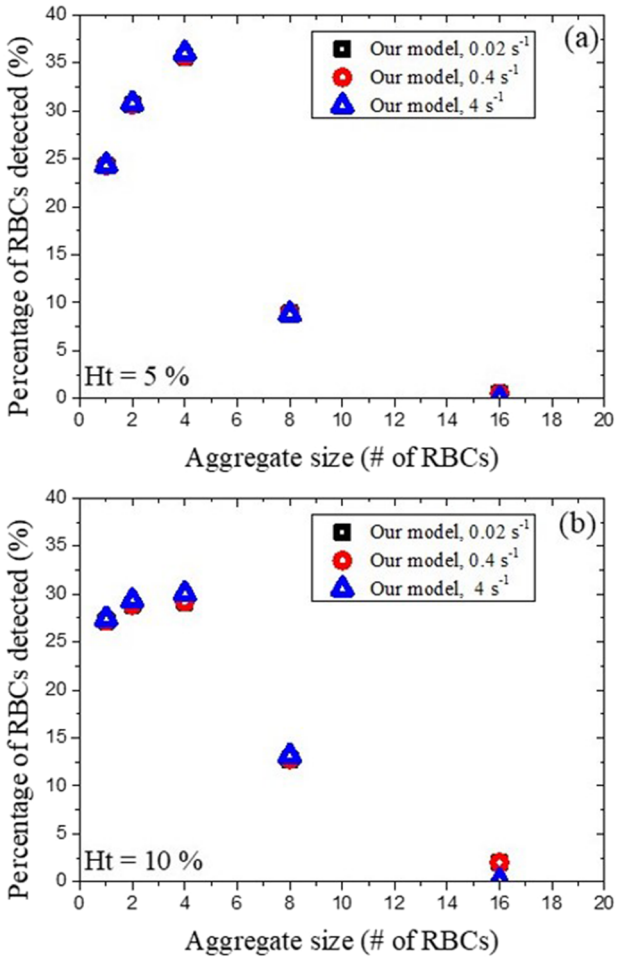

FIG. 5. Predictions of the model presented here for the rouleau size distribution using the same parameters as in Fig. 4 for the following conditions: (a) $Ht = 5\%$ at $\dot{\gamma} = 0.02$, 0.4, and 4 s^{-1}, and (b) $Ht = 10\%$ at $\dot{\gamma} = 0.02$, 0.4, and 4 s^{-1}.

VII. DISCUSSION AND CONCLUSIONS

We have derived a new constitutive model for the rheological behavior of blood guided by the work of Owens and co-workers (Owens, 2006; Fang and Owens, 2006; and Moyers-Gonzalez *et al.*, 2008) who relied on temporary network theory to model the formation and dissociation of rouleaux. The new model has been developed in the context of the generalized bracket formalism of nonequilibrium thermodynamics and accounts for the reversible formation and dissociation of rouleaux by incorporating a kinetic model (Germann *et al.*, 2013). Our approach suggests that the approximation made in the kinetic theory-based model of Owens and collaborators that the aggregation of RBCs is a Brownian process (and thus it stays always at equilibrium) is accurate only in the regime of small shear rates. Nevertheless, and despite their totally different starting points (one is based on polymer kinetic theory and the other is derived solely in the context of nonequilibrium thermodynamics), the overall similarity of our model with that of Owens' is striking; as a result, their predictions for the size distribution of rouleaux are also very similar.

The biggest difference between the new approach and the kinetic theory model of Owens is that the former leads self-consistently also to a closed set of algebraic equations for the aggregation and disaggregation rates (inherently related to the free energy expression) as a function of the applied flow strength and rouleau conformation [see Eqs. (7)]; this is very important since, through this, we avoid the need to resort to phenomenological approximations to specify these rates.

In addition to guaranteeing the thermodynamic admissibility and the internal consistency of the final transport equations (in the sense that aggregation/disaggregation rates are specified self-consistently), our approach further provides the necessary formalism in order to incorporate additional mechanisms that have been omitted in the version of the model presented here. We mention, in particular, stress gradient-induced migration and wall effects, which are absolutely necessary if one wishes to address phenomena such as the Fåhraeus and Fåhraeus-Lindqvist effects. The new approach provides also a nice framework for including different mechanistic descriptions of the rouleaux, such as the rigid-rod representation or even a description in terms of a continuous distribution of rouleau sizes. We also note here that if RBCs are not allowed to aggregate, then both the current model and the model by Owens predict a constant shear viscosity. But this contradicts many experimental data showing that by removing fibrinogen (which is responsible for the aggregation mechanism) blood progressively departs from the Newtonian behavior with increasing *Ht* (Chien *et al.*, 1966). To account for the elastic membrane enclosing the hemoglobin solution, single RBCs should be modeled as deformable emulsion droplets.

In the future, we would like to parameterize (and even refine) our model based on more detailed information obtained from independent DPD simulations [see, e.g., Fedosov *et al.* (2011) and Pan *et al.* (2010)] or direct experimental measurements for the evolving microstructure of rouleaux under normal human blood conditions, both for transient and steady flows. Very few researchers (Kaliviotis *et al.*, 2011 and Kaliviotis and Yianneskis, 2011) have studied experimentally the dynamics of rouleau formation under normal *Ht* conditions. And in their majority, these studies provide data only for the average rouleau size, which is not enough for the complete parameterization of the proposed model. We would also like to extend our model in the following aspects:

(1) To incorporate information about the dependence of its viscoelastic parameters on hematocrit and fibrinogen concentration.
(2) To pursue a representation of rouleaux in terms of rigid rods (rather than assuming them to be deformable dumbbells). In our approach, this can be easily accomplished by using as structural variable the orientation tensor **a** for the rouleaux (properly constrained to have a constant trace to account for the rather rigid configuration of the various rouleaux). A similar description has been followed recently (Stephanou *et al.*, 2014 and Stephanou, 2015) to derive a differential rheological model for polymer melt nanocomposites.
(3) To move from the simple and very approximate description in terms of rouleaux that have a specific size to a more general description in terms of a continuous distribution of rouleau sizes (Samsel and Perelson, 1982; 1984); it seems that this is a prerequisite for the correct

prediction of the dependence of the average rouleau size on the shear rate.

(4) To include terms accounting for stress-gradient induced migration of RBCs and rouleaux as well as to incorporate wall effects in order to address the Fåhraeus and Fåhraeus-Lindqvist effects. Accounting for cell-vessel interactions is a very challenging issue since it requires coupling of the generalized bracket formalism with a microscopic model for the proper description of these interactions. But some work already exists: for example, Mavrantzas and Beris (1999a; 1999b) have already proposed such a hierarchical modeling approach to address wall effects in flowing polymer solutions. Also, Öttinger (2008) has performed a similar study of wall effects for polymer melts within the context of the GENERIC formalism of nonequilibrium thermodynamics. As far as stress gradient-induced migration is concerned, this can be accounted for by resorting to a two-fluid model (Beris and Mavrantzas, 1994; Mavrantzas and Beris, 1999a; 1999b; and Apostolakis *et al.*, 2002) as in the case of inhomogeneous flows of polymer solutions.

SUPPLEMENTARY MATERIAL

See supplementary material for all technical issues related with the use of the generalized bracket formalism and the two brackets (the Poisson and the dissipation). A summary of the set of parameters involved in the Owens model is also provided.

ACKNOWLEDGMENTS

The authors would like to thank Professor A. N. Beris and Professor E. Kaliviotis for patiently answering many questions that we had on their published work on the rheology and mechanics of blood. We express our gratitude to Professor E. Kaliviotis for bringing to our attention the experimental data discussed in Fig. 4. This work was co-funded (a) by the Bodossaki Foundation by granting a M.Sc. scholarship to I. Ch. Tsimouri and (b) by the Republic of Cyprus through the Research Promotion Foundation (Project No. KOYLTOYRA/BP-NE/0415/01) granted to P. S. Stephanou through the "Cyprus Research Award-Young Researcher 2015" award.

Anand, M. and Rajagopal, K. R., "A shear-thinning viscoelastic fluid model for describing the flow of blood," Int. J. Cardiovasc. Med. Sci. **4**, 59–68 (2004).

Apostolakis, M. V., Mavrantzas, V. G., and Beris, A. N., "Stress gradient-induced migration effects in the Taylor-Couette flow of a dilute polymer solution," J. Non-Newton. Fluid Mech. **102**, 409–445 (2002).

Apostolidis, A. J. and Beris, A. N., "Modeling of the blood rheology in steady-state shear flows," J. Rheol. **58**, 607–633 (2014).

Barabino, G. A., Platt, M. O., and Kaul, D. K., "Sickle cell biomechanics," Annu. Rev. Biomed. Eng. **12**, 345–367 (2010).

Barshtein, G., Wajnblum, D., and Yedgar, S., "Kinetics of linear rouleaux formation studied by visual monitoring of red cell dynamic organization," Biophys. J. **78**, 2470–2474 (2000).

Baskurt, O. K. and Meiselman, H. J., "Blood rheology and hemodynamics," Semin. Thromb. Hemostasis **29**, 435–450 (2003).

Beris, A. N., "Simple non-equilibrium thermodynamics applications to polymer rheology," Rheol. Rev. **2003**, 37–75.

Beris, A. N. and Edwards, B. J., *Thermodynamics of Flowing Systems With Internal Microstructure* (Oxford University Press, New York, 1994).

Beris, A. N. and Mavrantzas, V. G., "On the compatibility between various macroscopic formalisms for the concentration and flow of dilute polymer solutions," J. Rheol. **38**, 1235 (1994).

Bureau, M., Healy, J. C., Bourgoin, D., and Joly, M., "Rheological hysteresis of blood at low shear rate," Biorheology **17**, 191–203 (1980).

Chen, S., Gavish, B., Mahler, Y., and Yedgar, S., "Monitoring of erythrocyte aggregate morphology under flow by computerized image analysis," Biorheology **32**, 487–496 (1995).

Chien, S., "Shear dependence of effective cell volume as a determinant of blood viscosity," Science **168**, 977–979 (1970).

Chien, S., Usami, S., Taylor, H. M., Lundberg, J. L., and Gregersen, M. I., "Effects of hematocrit and plasma proteins on human blood rheology at low shear rates," J. Appl. Physiol. **21**, 81–87 (1966).

Cho, Y. I., Mooney, M. P., and Cho, D. J., "Hemorheological disorders in diabetes mellitus," J. Diabetes Sci. Technol. **2**, 1130–1138 (2008).

Doi, M. and Edwards, S. F., *The Theory of Polymer Dynamics* (Oxford, Clarendon, United Kingdom, 1986).

Eckmann, D. M., Bowers, S., Stecker, M., and Cheung, A. T., "Hematocrit, volume expander, temperature, and shear rate effects on blood viscosity," Anesth. Analg. **91**, 539–545 (2000).

Fang, J. and Owens, R. G., "Numerical simulations of pulsatile blood flow using a new constitutive model," Biorheology **43**, 637–660 (2006).

Fedosov, D. A., Pan, W., Caswell, B., Gompper, G., and Karniadakis, G. E., "Predicting human blood viscosity in silico," Proc. Natl. Acad. Sci. U. S. A. **108**, 11772–11777 (2011).

Germann, N., Cook, L. P., and Beris, A. N., "Nonequilibrium thermodynamic modeling of the structure and rheology of concentrated wormlike micellar solutions," J. Non-Newton. Fluid Mech. **196**, 51–57 (2013).

Grmela, M. and Öttinger, H. C., "Dynamics and thermodynamics of complex fluids. I. Development of a general formalism," Phys. Rev. E **56**(6), 6620 (1997).

Herschel, W. H. and Bulkley, R., "Konsistenzmessungen von gummi benzollösungen," Kolloid-Z. **39**, 291–300 (1926).

Ju, M., Ye, S. S., Namgung, B., Cho, S., Low, H. T., Leo, H. L., and Kim, S., "A review of numerical methods for red blood cell flow simulation," Comput. Methods Biomech. Biomed. Eng. **18**, 130 (2013).

Kaestner, L., Steffen, P., Nguyen, D., Wang, J., Wagner-Britz, L., Jung, A., Wagner, C., and Bernhardt, I., "Lysophosphatidic acid induced red blood cell aggregation in vitro," Bioelectrochemistry **87**, 89–95 (2012).

Kaliviotis, E., "Mechanics of the red blood cell network," J. Cell. Biotechnol. **1**, 37–43 (2015).

Kaliviotis, E. and Yianneskis, M., "Fast response characteristics of red blood cell aggregation," Biorheology **45**, 639–649 (2008).

Kaliviotis, E. and Yianneskis, M., "Blood viscosity modelling: Influence of aggregate network dynamics under transient conditions," Biorheology **48**, 127–147 (2011).

Kaliviotis, E., Dusting, J., and Balabani, S., "Spatial variation of blood viscosity: Modelling using shear fields measured by a μPIV based technique," Med. Eng. Phys. **33**, 824–831 (2011).

Kaliviotis, E., Sherwood, J. M., and Balabani, S., "Partitioning of red blood cell aggregates in bifurcating microscale flows," Sci. Rep. **7**, 44563 (2017).

Mavrantzas, V. G. and Beris, A. N., "A hierarchical model for surface effects on chain conformation and rheology of polymer solutions. I. General formulation," J. Chem. Phys. **110**, 616–627 (1999a).

Mavrantzas, V. G. and Beris, A. N., "A hierarchical model for surface effects on chain conformation and rheology of polymer solutions. II. Application to a neutral surface," J. Chem. Phys. **110**, 628–638 (1999b).

Mehri, R., Laplante, J., Mavriplis, C., and Fenech, M., "Investigation of blood flow analysis and red blood cell aggregation," J. Med. Biol. Eng. **34**, 469–474 (2013).

Merrill, E. W. and Pelletier, G. A., "Viscosity of human blood: Transition from Newtonian to non-Newtonian," J. Appl. Physiol. **23**, 178–182 (1967).

Merrill, E. W., Gilliland, E. R., Cokelet, G., Shin, H., Britten, A., and Wells, R. E., Jr., "Rheology of human blood, near and at zero flow: Effects of temperature and hematocrit level," Biophys. J. **3**, 199–213 (1963a).

Merrill, E. W., Cokelet, G. C., Britten, A., and Wells, R. E., Jr., "Non-Newtonian rheology of human-blood-effect of fibrinogen deduced by 'subtraction'," Circ. Res. **13**, 48–55 (1963b).

Merrill, E. W., Benis, A. M., Gilliland, E. R., Sherwood, T. K., and Salzman, E. W., "Pressure-flow relations of human blood in hollow fibers at low flow rates," J. Appl. Physiol. **20**, 954–967 (1965).

Moyers-Gonzalez, M., Owens, R. G., and Fang, J., "A non-homogeneous constitutive model for human blood. Part 1. Model derivation and steady flow," J. Fluid Mech. **617**, 327–354 (2008).
Murata, T. and Secomb, T. W., "Effects of shear rate on rouleau formation in simple shear flow," Biorheology **25**, 113–122 (1988).
Oldroyd, J. G., "On the formulation of rheological equations of state," Proc. R. Soc. A **200**, 523–541 (1950).
Öttinger, H. C., *Beyond Equilibrium Thermodynamics* (Wiley-Interscience, New York, 2004).
Öttinger, H. C., "Thermodynamic formulation of wall slip," J. Non-Newtonian Fluid Mech. **152**, 66–75 (2008).
Öttinger, H. C. and Grmela, M., "Dynamics and thermodynamics of complex fluids. II. Illustrations of a general formalism," Phys. Rev. E **56**(6), 6633 (1997).
Owens, R. G., "A new microstructure-based constitutive model for human blood," J. Non-Newtonian Fluid Mech. **140**, 57–70 (2006).
Pan, W., Caswell, B., and Karniadakis, G. E., "A low-dimensional model for the red blood cell," Soft Matter **6**, 4366–4376 (2010).
Perkkiö, J. and Keskinen, R., "Hematocrit reduction in bifurcations due to plasma skimming," Bull. Math. Biol. **45**(1), 41–50 (1983).
Rajagopal, K. R. and Srinivasa, A. R., "A thermodynamic frame work for rate type fluid models," J. Non-Newtonian Fluid Mech. **88**, 207–227 (2000).
Samsel, R. W. and Perelson, A. S., "Kinetics of rouleau formation. I. A mass action approach with geometric features," Biophys. J. **37**, 493–514 (1982).
Samsel, R. W. and Perelson, A. S., "Kinetics of rouleau formation. II. Reversible reactions," Biophys. J. **45**, 805–824 (1984).
Schmid Schönbein, H., Gaehtgens, P., and Hirsch, H., "On the shear rate dependence of red cell aggregation in vitro," J. Clin. Invest. **47**, 1447–1454 (1968).
Shalak, R., Keller, S. R., and Secomb, T. W., "Mechanics of blood flow," J. Biomech. Eng. **103**, 102–115 (1981).
Shelby, J. P., White, J., Ganesan, K., Rathod, P. K., and Chiu, D. T., "A microfluidic model for single-cell capillary obstruction by Plasmodium falciparum-infected erythrocytes," Proc. Natl. Acad. Sci. U. S. A. **100**, 14618–14622 (2003).
Shiga, T., Imaizumi, K., Harada, N., and Sekiya, M., "Kinetics of rouleaux formation using TV image analyzer. I. Human erythrocytes," Am. J. Physiol. **245**, H252–H258 (1983a).
Shiga, T., Imaizumi, K., Maeda, N., and Kon, K., "Kinetics of rouleaux formation using TV image analyzer. II. Rat erythrocytes," Am. J. Physiol. **245**, H259–H264 (1983b).
Steffen, P., Verdier, C., and Wagner, C., "Quantification of depletion-induced adhesion of red blood cells," Phys. Rev. Lett. **110**, 018102 (2013).
Stephanou, P. S., "How the flow affects the phase behaviour and microstructure of polymer nanocomposites," J. Chem. Phys. **142**, 064901 (2015).
Stephanou, P. S., "The rheology of drilling fluids from a non-equilibrium thermodynamics perspective," J. Pet. Sci. Eng. (published online 2017).
Stephanou, P. S., Baig, C., and Mavrantzas, V. G., "A generalized differential constitutive equation for polymer melts based on principles of nonequilibrium thermodynamics," J. Rheol. **53**, 309–337 (2009).
Stephanou, P. S., Mavrantzas, V. G., and Georgiou, G. C., "Continuum model for the phase behavior, microstructure, and rheology of unentangled polymer nanocomposite melts," Macromolecules **47**, 4493–4513 (2014).
Stephanou, P. S., Tsimouri, I. Ch., and Mavrantzas, V. G., "Flow-induced orientation and stretching of entangled polymers in the framework of nonequilibrium thermodynamics," Macromolecules **49**, 3161–3173 (2016).
Szołna-Chodór, A., Bosek, M., and Grzegorzewski, B., "Kinetics of red blood cell rouleaux formation studied by light scattering," J. Biomed. Opt. **20**(2), 025001 (2015).
Usmani, R., "Inversion of a tridiagonal jacobi matrix," Linear Algebra Appl. **212-213**, 413–414 (1994).
Usami, S., Chien, S., and Bertles, J. F., "Deformability of sickle cells as studied by micro-sieving," J. Lab. Clin. Med. **86**, 274–279 (1975).
Yilmaz, F. and Gundogdu, M. Y., "A critical review on blood flow in large arteries; relevance to blood rheology, viscosity models, and physiologic conditions," Korea-Australia Rheol. J. **20**, 197–211 (2008).